Spectroscopy of the $(\alpha, 2\alpha)$ reaction at $E_\alpha = 90$ MeV †

Joseph D. Sherman,* D. L. Hendrie, and M. S. Zisman
University of California, Lawrence Berkeley Laboratory, Berkeley, California 94720
(Received 15 September 1975)

Nine target nuclei ^{12}C, ^{16}O, ^{24,26}Mg, ^{28,30}Si, ^{40,44}Ca, and ^{66}Zn have been studied by the $(\alpha, 2\alpha)$ reaction at an incident beam energy of 90 MeV. Energy resolution of 250–300 keV full width at half-maximum permitted identification of many excited states, although transitions to the ground state consistently dominated the spectra. The ground state angular correlations for equal outgoing energies and angles were similar in shape over this mass region although the magnitude decreased by a factor of 10 from ^{12}C to ^{66}Zn. A phenomenological distorted wave impulse approximation calculation successfully describes most of the angular and energy correlations. A conspicuous failure of the calculation occurs in the energy correlation predictions for recoil momenta greater than 0.6 fm^{-1}. Spectroscopic results are compared with those from α pickup reactions. It is seen that both reactions give nearly the same α clustering mass dependence. Plane wave impulse approximation analysis suggests that the principle parent of ^{16}O in an α particle model is the ^{12}C ground state rather than the first excited state as found in the α pickup reactions.

PACS numbers:

[NUCLEAR REACTIONS ^{12}C, ^{16}O, ^{24,26}Mg, ^{28,30}Si, ^{40,44}Ca, ^{66}Zn $(\alpha, 2\alpha)$, $E_\alpha = 90$ MeV, measured energy and angular correlations; DWIA, PWIA analysis, α cluster spectroscopy.]

I. INTRODUCTION

The object of this work was to investigate the $(\alpha, 2\alpha)$ reaction at 90 MeV incident α energy as a probe sensitive to α clustering in light and medium mass nuclei. The nine targets ^{12}C, ^{16}O, ^{24,26}Mg, ^{28,30}Si, ^{40,44}Ca, and ^{66}Zn were studied at several symmetric coplanar angle pairs. Asymmetric coplanar angle pairs were also taken for the ^{12}C and ^{16}O targets in order to clarify certain aspects of the reaction mechanism as well as provide further data concerning the spectroscopy of these nuclei. The extracted angular and energy correlations are reasonably consistent with an impulse approximation description of the reaction.

Several recent $(\alpha, 2\alpha)$ experiments on light nuclei (particularly ^{6}Li) in the 40 MeV to 70 MeV incident α energy range have used the plane wave impulse approximation (PWIA) in interpreting the data.[1,2] The PWIA analysis of the ^{6}Li$(\alpha, 2\alpha)$ reaction[2] required the use of a radial cutoff to obtain the best agreement with experimental results, which indicated that absorption effects were important. In order to analyze the present $(\alpha, 2\alpha)$ experiments, a parametrized distorted wave impulse approximation (DWIA) was derived. The distorted waves were represented by McCarthy-Pursey wave functions[3] with the focus term set to zero. This DWIA model described several systematic features of the $(\alpha, 2\alpha)$ reactions without invoking a radial cutoff in the bound state wave function. A spectroscopic factor has been defined which yields results in substantial agreement with a distorted wave Born approximation (DWBA) analysis of a systematic (^{3}He, ^{7}Be) study.[4] Spectroscopic information from a PWIA analysis[2,5,6] is also presented.

The $(\alpha, 2\alpha)$ reaction has also been studied on a ^{20}Ne target at $E_\alpha = 78.6$ MeV,[7] and on ^{12}C, ^{16}O, ^{26}Mg, and ^{28}Si, targets at $E_\alpha = 70$ MeV.[8] These data also display features of α-α quasielastic scattering, and a consistent picture of the $(\alpha, 2\alpha)$ reaction on nuclei removed from the p shell is beginning to develop.

The following section gives a summary of the theory. The third section describes the experiment, and the fourth section gives the analysis of the experimental results within the DWIA and PWIA frameworks. A comparison with α pickup reactions is also given in this part. The final section summarizes and discusses the results.

II. THEORY

A general discussion of the DWIA and PWIA used in analyzing the $(\alpha, 2\alpha)$ data is given here. The notation utilized is that the incident α particle labeled (1) is in the z direction and strikes the target nucleus $(2 + c)$ where 2 is the initially bound α particle and c the core. Two α particles (3 and 4) appear in the final state, and the residual nucleus (c) recoils. The experiment was arranged to be most sensitive to particles 3 and 4 having large velocities, while the recoil nucleus received only a small impulse. Figure 1 depicts the kinematics

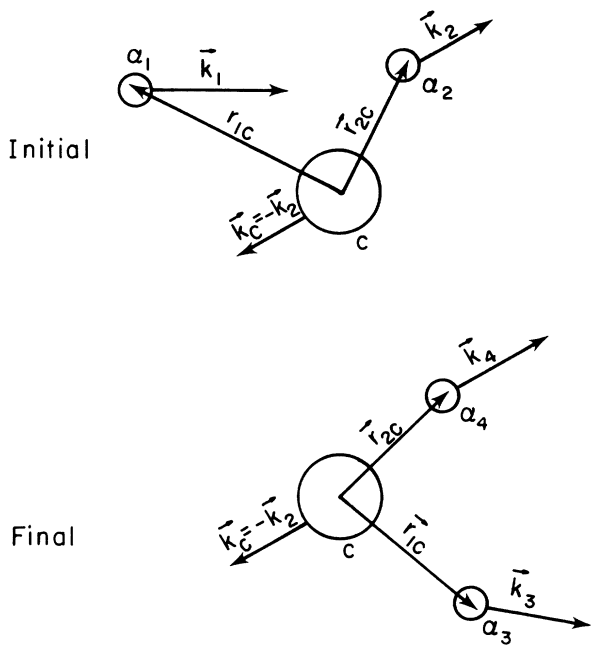

FIG. 1. Coordinate system used in the $(\alpha, 2\alpha)$ theory. The core is represented by c. The incident α particle is labeled 1 and the initially bound α particle is 2. In the final state 3 and 4 represent the two product α particles.

in the initial and final states; the core is assumed to be infinitely massive (no recoil) and also centered at the origin of the reference frame. Conservation of momentum and kinetic energy in the lab frame yields

$$\vec{k}_1 + \vec{k}_2 + \vec{k}_c = \vec{k}_3 + \vec{k}_4 + \vec{k}_c \tag{1}$$

and

$$E_1 + Q = E_3 + E_4 + E_c\,, \tag{2}$$

where the $\vec{k}_i$ $(=\vec{p}_i/\hbar)$ are wave numbers and the E_i are kinetic energies. The quantity Q is the binding energy of an α particle in the target nucleus. Since the target is at rest in the lab frame $\vec{k}_2 + \vec{k}_c = 0$. Further, $\vec{k}_2 = \vec{q} = -\vec{k}_c$ where $\vec{q}$ is the momentum of the initially bound α particle.

A general statement for the three body cross section in terms of the T matrix is[9]

$$d^3\sigma = \frac{2\pi}{\hbar v_1} \sum_M |T_L^M(\vec{k}_1, \vec{k}_3, \vec{k}_4)|^2 \rho_f(E_1)\,, \tag{3}$$

where T_L^M (the arguments of T_L^M are suppressed in what follows) is a T matrix element and $\rho_f(E_1)$ is a phase space factor.[10,11] In a plane wave Born approximation treatment the T_L^M can be written[12]

$$T_L^M = \int e^{i\vec{k}_1\cdot\vec{r}_{1c}} f_{NL}^M(\vec{r}_{2c}) V(|\vec{r}_{1c} - \vec{r}_{2c}|) \times e^{-i\vec{k}_3\cdot\vec{r}_{1c}} e^{-i\vec{k}_4\cdot\vec{r}_{2c}} d\vec{r}_{1c} d\vec{r}_{2c}\,, \tag{4}$$

where the incident α $(\vec{r}_{1c}, \vec{k}_1)$ interacts with the second α bound to the core of mass $A-4$ with the wave function $f_{NL}^M(\vec{r}_{2c})$ via the interaction $V(|\vec{r}_{1c} - \vec{r}_{2c}|)$. Since exchange effects are not included, the two outgoing α particles are described, respectively, with $(\vec{r}_{1c}, \vec{k}_3)$ and $(\vec{r}_{2c}, \vec{k}_4)$. It is noted that recoil effects have been neglected in Eq. (4). (See Fig. 1.)

Using the coordinate transformations[12]

$$\vec{r} = \vec{r}_{1c} - \vec{r}_{2c}, \quad \vec{\rho} = \vec{r}_{2c}\,, \tag{5}$$

the T_L^M of Eq. (4) reduces to the product of two integrals

$$T_L^M = \int d\vec{r} \exp[i(\vec{k}_1 - \vec{k}_3)\cdot\vec{r}\,] V(|\vec{r}|) \times \int d\vec{\rho} \exp[i\vec{k}_c\cdot\vec{\rho}\,] f_{NL}^M(\vec{\rho})\,. \tag{6}$$

In the impulse approximation the first integral of Eq. (6) is replaced with an appropriate free α-α scattering cross section,[13] and the PWIA results. The second integral of Eq. (6) is the Fourier transform of the bound α particles coordinate space wave function $[f_{NL}^M(\vec{\rho})]$ with respect to the momentum of the recoiling nucleus. The square of this integral describes the momentum distribution of the particle.[14]

For nonzero Q, the momentum transferred by the scattered α particle, $\vec{k}_1 - \vec{k}_3$, is not the same (for a fixed incident energy and scattering angle) in the $(\alpha, 2\alpha)$ reaction as it is for free (α, α) scattering. This off-the-mass-shell effect requires careful selection of an (α, α) scattering energy to be appropriate for the reaction. This will be discussed in Sec. IV B in conjunction with the data.

If the three plane waves of the second integral in Eq. (6) are replaced by more realistic distorted waves,[3,15] but the impulse approximation is maintained, the DWIA is obtained and the second integral is written as

$$\Phi_{NL}^M(\vec{\xi}) = \int_{-\infty}^{+\infty} d\vec{\rho}\, \chi^{*(-)}(\vec{k}_4, \vec{\rho}) \chi^{*(-)}(\vec{k}_3, \vec{\rho}) f_{NL}^M(\vec{\rho}) \times \chi^{(+)}(\vec{k}_1, \vec{\rho})\,, \tag{7}$$

where the $\chi^{(+)}$ $(\chi^{*(-)})$ are incoming (outgoing) distorted waves. The complex variable $\vec{\xi}$ will be defined below. The χ's in Eq. (7) are taken to be the analytic distorted waves of the McCarthy-Pursey type.[3] Early work in treating inelastic α particle scattering data with the McCarthy-Pursey parametrized distorted waves showed that the focus term makes a small contribution compared to the surface term,[3] so the focus term was dropped in our treatment. The full parametrization has been kept in $(p, 2p)$ calculations.[16]

The McCarthy-Pursey distorted waves are de-

TABLE I. The first three columns give target information. The final three columns concern the radial wave function of an α particle bound in the various targets studied in this work.

Target	Isotopic purity	Thickness (mg/cm^2)	α-particle separation energy (MeV)	Radial nodes N	Binding potential (MeV)
^{12}C	Natural	0.379 ± 0.010	7.369	2	68.8
^{16}O(NiO)	Natural	0.255 ± 0.050	7.161	2	60.9
^{24}Mg	99% ^{24}Mg	1.075 ± 0.040	9.316	4	109.5
^{26}Mg	99% ^{26}Mg	0.435 ± 0.020	10.614	4	106.9
^{28}Si	Natural	0.692 ± 0.020	9.981	4	104.1
^{30}Si	89% ^{30}Si 10% ^{28}Si	0.076 ± 0.015	10.650	4	100.9
^{40}Ca	Natural	0.457 ± 0.090	7.041	4	87.5
^{44}Ca	98.5% ^{44}Ca	0.420 ± 0.020	8.846	5	109.4
^{66}Zn	97.8% ^{66}Zn	0.586 ± 0.060	4.558	6	109.2

scribed in the initial channel by

$$\chi^{(+)}(\vec{k}_1, \vec{\rho}) = N_1 \exp[i(\beta_1 + i\gamma_1/(k_1 R_s))\vec{k}_1 \cdot \vec{\rho}] \quad (8)$$

and final channels by

$$\chi^{*(-)}(\vec{k}_3, \vec{\rho}) = N_3 \exp[-i(\beta_3 + i\gamma_3/(k_3 R_s))\vec{k}_3 \cdot \vec{\rho}] \quad (9)$$

and similarly for $\chi^{*(-)}(\vec{k}_4, \vec{\rho})$. Here N_1, N_3, and N_4 are normalization factors derived from the condition that the magnitude of the distorted waves at $\rho = 0$ is $\exp(-\gamma_i)$ for $i = 1$, 3, and 4.[17] The nuclear radius parameter R_s is taken to be $1.30A^{1/3}$ in the initial channel and $1.30(A-4)^{1/3}$ in the final channel, where A is the mass of the target nucleus. The β and γ parameters can be estimated[16] from standard optical model potential parameters by

$$\beta_i = \left(\frac{E_i - V}{E_i}\right)^{1/2}, \quad (10)$$

$$\gamma_i = R_s\left[\left(\frac{\mu}{2\hbar^2}\right)\frac{W^2}{E_i - V}\right]^{1/2}. \quad (11)$$

the quantities V, W, and μ are the real and imaginary parts of the optical model potential and the reduced mass of the system. The β parameter relates the asymptotic wave number (k) to a local wave number (βk), and for $V < 0$ (attractive potential) β is greater than unity. The γ parameter measures absorption of the incident and scattered waves.

Use of Eqs. (8) and (9) in Eq. (7) would, in principle, require the determination of six parameters to fully specify the distorted waves. However, in our analysis the final state distortion parameters have been set equal because the present experiments are performed so that the two product α particles have roughly equal energies. These final state distortion parameters are denoted $\beta_{3,4}$ and $\gamma_{3,4}$. Thus the two complex numbers α_1 and $\alpha_{3,4}$

$$\alpha_1 = \beta_1 + i\gamma_1/(k_1 R_s) \quad (12)$$

and

$$\alpha_{3,4} = \beta_{3,4} + i\gamma_{3,4}/(k_{3,4} R_s) \quad (13)$$

define the distorted waves in the initial and final channels. Considering only the knockout of an $L = 0$ α particle, we obtain substituting $\chi^{(+)}$ and $\chi^{*(-)}$ into Eq. (7)

$$\phi^0_{N0}(\vec{\xi}) = N_1 (N_{3,4})^2 \int_{-\infty}^{+\infty} e^{i\vec{\xi}\cdot\vec{\rho}} f^0_{N0}(\vec{\rho})\, d\vec{\rho}, \quad (14)$$

where

$$\vec{\xi} = \alpha_1 \vec{k}_1 - \alpha_{3,4}(\vec{k}_3 + \vec{k}_4). \quad (15)$$

In the plane wave limit, β_1 and $\beta_{3,4}$ equal unity and γ_1 and $\gamma_{3,4}$ equal zero; $\vec{\xi}$ in this case equals the recoil momentum $\vec{k}_c$, and the plane wave result is recovered.

The wave function for an α-particle cluster bound to the core with relative angular momentum (L) equal to zero is

$$f_{N0}(\vec{\rho}) = (S_\alpha{}^{1/2})_{DW} \frac{R_{N0}(\rho)}{\sqrt{4\pi}}, \quad (16)$$

where $(S_\alpha{}^{1/2})_{DW}$ is an α cluster spectroscopic factor and $R_{N0}(\rho)$ is the relative radial wave function between the bound cluster and core. The quantum number N is the number of radial nodes in $R_{N0}(\rho)$ and is derived from consideration of energy conservation within the harmonic oscillator shell model[18,19] by use of the relation

$$\sum_{i=1}^{A} (2n_i + l_i) = 2N + L + \sum_{c=1}^{A-4} (2n_c + l_c), \quad (17)$$

where it is assumed that the α cluster is composed of four valence nucleons outside the core c. For $L = 0$ and assuming the valence shell model particles are active in clustering, N is derived from Eq. (17) and tabulated in Table I. The subscript

TABLE II. Summary of the collimator sizes used in this work.

Set	Detector	Solid angle (msr)	Radii (cm)	Angular radial acceptance (deg)	Angular vertical acceptance (deg)
A	1	4.70	4.29	2.11	±3.73
	2	4.60	4.22	1.96	±3.73
B	1	1.40	7.85	1.15	±2.09
	2	1.46	7.47	1.09	±2.09

DW attached to $(S_\alpha{}^{1/2})_{DW}$ indicates the spectroscopic factor was extracted from the DWIA theory.

III. EXPERIMENTAL

The experiment was done with a magnetically analyzed[20] 90 MeV α beam with $\Delta E/E = 8 \times 10^{-4}$ from the Berkeley 88 in. cyclotron. The energy was sufficient to separate sequential α decay events arising from discrete (resolved) levels in intermediate nuclei from quasielastic events. These latter events have maximum cross section when the energy is equally shared between the two outgoing α particles, while the sequential processes would normally lead to an asymmetric distribution.

The data were taken in a 91 cm scattering chamber in which two independently controlled counter arms were mounted. Each arm held a detector telescope which consisted of a 250 μm phosphorus diffused Si transmission detector and a 3 mm Si(Li) stopping detector cooled to about $-25\,^\circ$C with thermoelectric devices. Electrons were suppressed by ~1.5 mg/cm^2 Al foils placed in front of the rectangular collimators. Table II summarizes the acceptance angles used in these experiments; Set A was used in the symmetric angle range of 28° to 47° and the asymmetric angle data, while Set B was used for the forward angle work. The effects of large solid angles were compensated by averaging the theoretical predictions over the radial acceptance angles. No correction was made for noncoplanar effects which are expected to be most important in the knockout of a particle with nonzero angular momentum.[21,22]

The electronic systems used high rate components designed by Goulding, Landis, and Pehl[23] and the logic is summarized in Fig. 2. The pileup rejectors (PUR) would typically give 10% dead time at a singles count rate of 15 000 sec^{-1}; they made the major contributions to experimental dead time. Inclusion of the PUR in the ΔE counting system gave an improvement of a factor of 3 for the elastically scattered α particle peak-to-valley ratio. The single channel analyzers (SCAs) on the ΔE counters were sufficient to select particles with Z equal to 2. The $(\alpha, \alpha\,{}^3\mathrm{He})$ events were separated by their large negative Q values. The fast coincidence spectrum was obtained by using a time-to-amplitude converter (TAC) triggered by the ΔE detectors. The time range of the TAC was 1 μs, giving eight chance peaks and one true plus chance peak in the time spectrum. The time resolution was 6 or 7 ns, well within the cyclotron period of about 100 ns.

The data were stored event by event by use of a multiplexer-ADC system[24] and a PDP-5 on-line computer. Each event was required to satisfy all timing and energy requirements; consequently, the count rate was in the range from one to ten events per second. For each event three pieces of information were stored: the two summed energy signals and the TAC signal. The data were subsequently analyzed off line with the TAC spectrum used to separate true plus chance and chance information into different arrays. This method permitted simultaneous accumulation of chance information with the true events; the analysis included the subtraction of a chance array from the true plus chance events. The total dead time of the electronic system was measured by injecting pulser signals which simulated α particles into the preamplifiers. The pulser unit was triggered by a

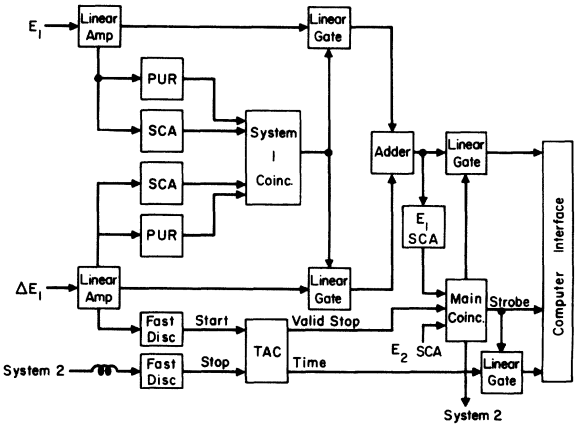

FIG. 2. Schematic of the electronics used in the coincidence counting. PUR is a pileup rejector, SCA is a single channel analyzer, and TAC is a time-to-amplitude converter.

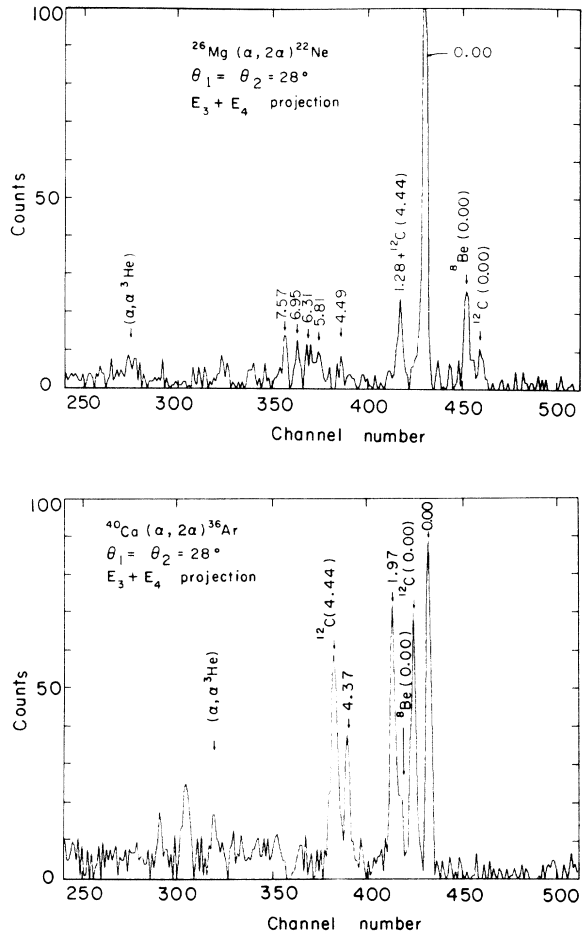

FIG. 3. Representative $E_3 + E_4$ projected spectra from the ^{26}Mg$(\alpha, 2\alpha)$ and ^{40}Ca$(\alpha, 2\alpha)$ reactions.

monitor counter. These signals progressed through the circuit exactly as a real coincident event and were eventually written on magnetic tape. By comparing the integrated pulser counts found on the data tapes with the number of monitor pulser triggers, the total dead time, varying from 10 to 30%, was measured. The monitor counter was also used to check for target deterioration and to verify the beam charge accumulated in a Faraday cup.

A summary of target information is included in Table I. Whenever possible, target thicknesses were measured by two techniques. First, the energy loss of 8.78 MeV α particles was measured, and second, a direct weighing of the target was made on a microgram balance. Careful choice of target thickness as well as the previously discussed experimental parameters resulted in 250–300 keV energy resolution in the $E_3 + E_4$ projected spectra (see Fig. 3). The energy scales were calibrated by observing the ^{12}C$(\alpha, \alpha')^{12}$C singles reaction as a function of angle. The error in this procedure was about $\frac{1}{2}$ channel, which yields about 1.5 MeV uncertainty in the E_3 scale.

IV. RESULTS AND DISCUSSION

A. Experimental results

Table III summarizes the residual levels observed in this $(\alpha, 2\alpha)$ survey. The second column gives the excitation energies obtained from the summed energy $(E_3 + E_4)$ spectra. These energies can be compared with the literature values given in the fourth column; the J^π values are also taken from the literature. Figure 3 shows sample ^{26}Mg$(\alpha, 2\alpha)$ and ^{40}Ca$(\alpha, 2\alpha)$ summed energy spectra; the $(\alpha, \alpha^3\text{He})$ thresholds are indicated. The final columns of Table III give information on the experimental intensities. Cross sections integrated over approximately 24 to 65 MeV in E_3 are given for data in which both counters had the angle θ. The errors reflect only the statistical uncertainties. It is seen that, with the exceptions of the ^{36}Ar and ^{8}Be residual nuclei, the ground state

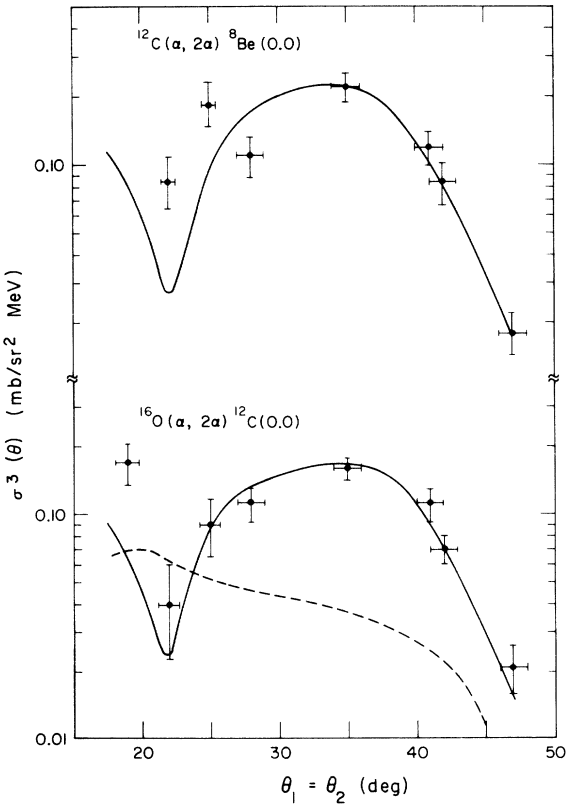

FIG. 4. Symmetric angular correlations for the ^{12}C$(\alpha, 2\alpha)^{8}$Be(0.0) and ^{16}O$(\alpha, 2\alpha)^{12}$C(0.0) reactions. The dashed curve is the $(E_{\alpha\alpha})_i$ prescription, while the solid curves are calculated on the basis of the $(E_{\alpha\alpha})_f$ method for extracting the $\alpha_{\alpha\alpha}(E_{\alpha\alpha}, \theta)$.

TABLE III. Residual levels populated by the $(\alpha, 2\alpha)$ reaction, as well as comparisons to literature excitations and a summary of experimental transition intensities obtained at the quoted angle.

Residual Nucleus	$E_{exc.}$ (MeV)	Error (keV)	$E_{lit.}$ (MeV)	Lit. J^π	θ (deg)	Integrated cross sections (mb/sr^2)
^{8}Be	0.00	•••	0.00 [a]	0^+ [a]	35	4.89 ±0.34
	2.90	•••	2.90	2^+		2.54 ±0.25
^{12}C	0.00	•••	0.00 [b]	0^+ [b]	35	3.41 ±0.35
	4.44	•••	4.439	2^+		0.88 ±0.17
	7.65	•••	7.653	0^+		Weak
^{20}Ne	0.00	±20	0.00 [c]	0^+ [c]	35	1.31 ±0.15
	1.63	±35	1.63	2^+		0.108 ± 0.042
	4.25	±60	4.25	4^+		Weak
	5.70	±60	5.62, 5.79	$3^-, 1^-$		0.063 ± 0.031
	6.72	±50	6.72	0^+		0.065 ± 0.028
	11.41	±50	Many levels			0.039 ± 0.022
^{22}Ne	0.00	±50	0.00 [d]	0^+ [d]	35	1.03 ±0.12
	1.28	±60	1.28	2^+		0.16 ±0.05
	4.49	±80	4.46	2^+		0.025 ± 0.018
	5.81	±60	5.93	–		0.018 ± 0.014
	6.31	±80	6.34	6^+		0.052 ± 0.024
	6.95	±150	6.90	0^+		0.030 ± 0.016
	7.57	±60	7.49, 7.64	$1^-, 2^+$		0.059 ± 0.026
^{24}Mg	0.00	±20	0.00 [e]	0^+ [e]	35	0.84 ±0.11
	1.37	±40	1.369	2^+		0.156 ± 0.047
	4.23	±30	4 123, 4.23	$4^+, 2^+$		Weak
	5.23	±70	5.228	3^+		0.033 ± 0.020
	7.69	±50	Several levels			0.040 ± 0.023
	11.47	±50	Many levels			0.045 ± 0.021
^{26}Mg	0.00	±50	0.00 [e]	0^+ [e]	35	0.61 ±0.16
	1.81	±50	1.809	2^+		0.12 ±0.07
	2.92	±100	2.938	2^+		Weak
	3.53	±100	3.585	0^+		Weak
^{36}Ar	0.00	±40	0.00 [e]	0^+ [e]	32	0.50 ±0.089
	1.97	±30	1.970	2^+		0.30 ±0.070
	4.37	±100	Several levels			0.10 ±0.039
^{40}Ar	0.00	±80	0.00 [e]	0^+ [e]	28	0.58 ±0.12
	1.44	±50	1.460	2^+		0.027 ± 0.032
	2.09	±90	2.125	0^+		0.052 ± 0.034
	4.00	±40	Several levels			0.080 ± 0.044
	5.75	±70	Several levels			0.026 ± 0.025
^{62}Ni	0.00	±30	0.00 [f]	0^+ [f]	35	0.42 ±0.071
	1.17	±40	1.172	2^+		0.062 ±0.026
	2.36	±100	2.303, 2.34	$2^+, 4^+$		Weak

[a] T. Lauritson and F. Ajzenberg-Selove, Nucl. Phys. 78, 1 (1966).
[b] F. Ajzenberg-Selove and T. Lauritson, Nucl. Phys. A114, 1 (1968).
[c] F. Ajzenberg-Selove, Nucl. Phys. A190, 1 (1972).
[d] W. Scholz, P. Neogy, K. Bethge, and R. Middleton, Phys. Rev. C 6, 893 (1972); P. Neogy, R. Middleton, and W. Scholz, *ibid.* 6, 885 (1972).
[e] P. M. Endt and C. Van Der Leun, Nucl. Phys. A105, 1 (1967).
[f] C. M. Lederer, J. M. Hollander, and I. Perlman, *Table of Isotopes* (Wiley, New York, 1967), 6th ed.

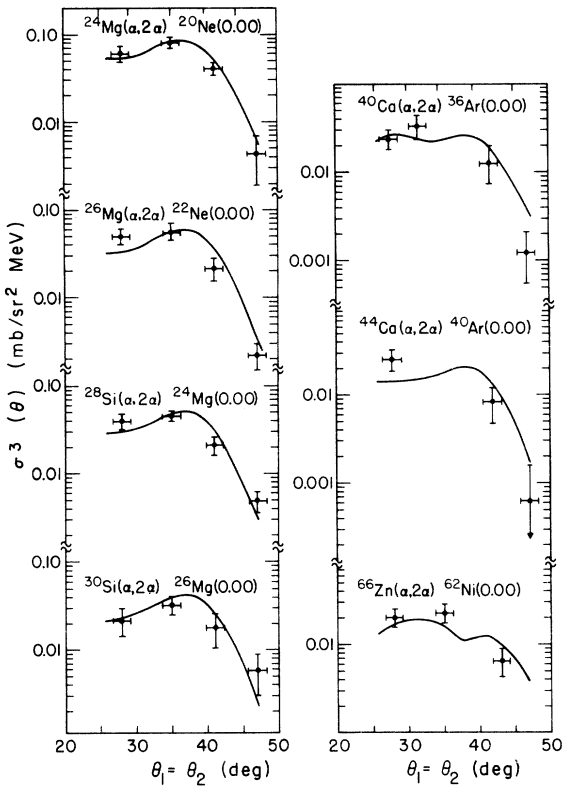

FIG. 5. Ground state transition $(\alpha, 2\alpha)$ symmetric angular correlations on the ^{24,26}Mg, ^{28,30}Si, ^{40,44}Ca, and ^{66}Zn targets. The solid curves are DWIA calculations.

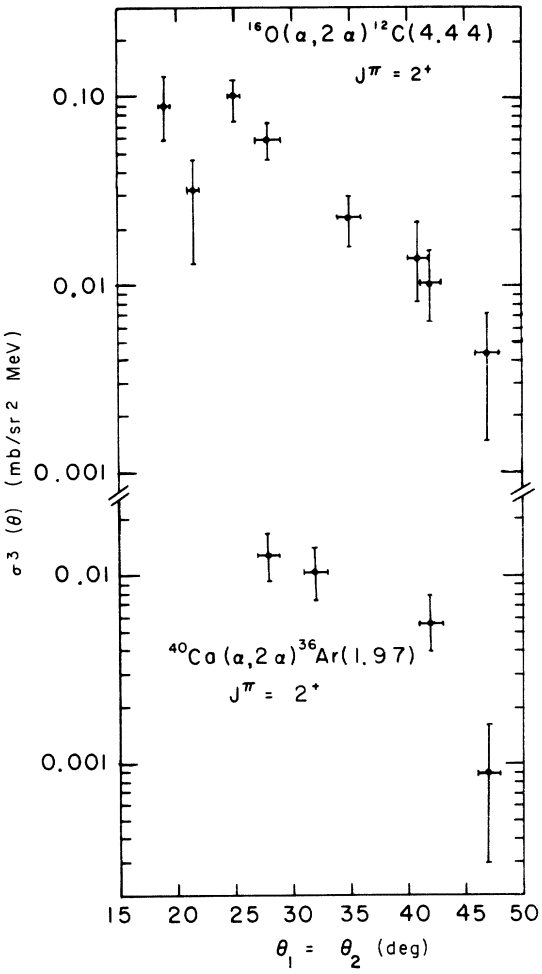

FIG. 6. Symmetric angular correlations for the first excited states in ^{12}C and ^{36}Ar from the ^{16}O$(\alpha, 2\alpha)^{12}$C-(4.44) and ^{40}Ca$(\alpha, 2\alpha)^{36}$Ar(1.97) reactions.

transitions strongly dominate. The ^{28}Si$(\alpha, 2\alpha)$ result disagrees with an earlier ^{28}Si$(\alpha, 2\alpha)$ experiment[25] at 104 MeV. The ^{28}Si$(\alpha, 2\alpha)$ reaction at $E_\alpha = 70$ MeV also finds the ^{24}Mg ground state most strongly populated,[8] in agreement with our data. Finally, the intensities are seen to decrease by an order of magnitude from ^{8}Be to ^{62}Ni.

Figures 4 through 7 present a selection of angular correlations measured in this work. Symmetric angular correlations ($\theta_1 = \theta_2$) for the ground state transitions are shown in Figs. 4 and 5, while Fig. 6 is a sample of such data to the first excited, $J^\pi = 2^+$ states. Figure 7 presents asymmetric angular correlation measurements (θ_1 fixed) obtained for ^{8}Be(0.0) and ^{12}C(0.0). The angular correlation data are averaged cross sections taken at the E_3 point in the energy correlation which required the residual nucleus recoil momentum to lie along the beam axis. The vertical error bars are statistical errors, and the horizontal error bars indicate experimental angular acceptances. Figures 8 and 9 show the ^{16}O$(\alpha, 2\alpha)^{12}$C(0.0) and ^{24}Mg$(\alpha, 2\alpha)^{20}$Ne(0.0) energy correlations as a function of symmetric scattering angle; the arrows in these figures show the point at which $E_3 = E_4$. Figure 10 shows the energy correlations for all targets at the symmetric angle pair for which the residual nucleus may have zero recoil momentum (the quasielastic angle). The set of three arrows in this figure show the points at which $|\vec{q}| \simeq 0.6$ fm^{-1} and $|\vec{q}| \simeq 0.0$ fm^{-1}. The uncertainty of the absolute cross section is estimated to be ±15%; the relative uncertainties are determined mainly by the precision of the target thickness measurements. Tabulations of the data can be found in Ref. 26. The solid curves are DWIA calculations to be discussed in the following sections.

B. DWIA reaction model

1. Choice of free α-α scattering cross sections

Using the equations developed in Sec. II, Eq. (1) may be rewritten as

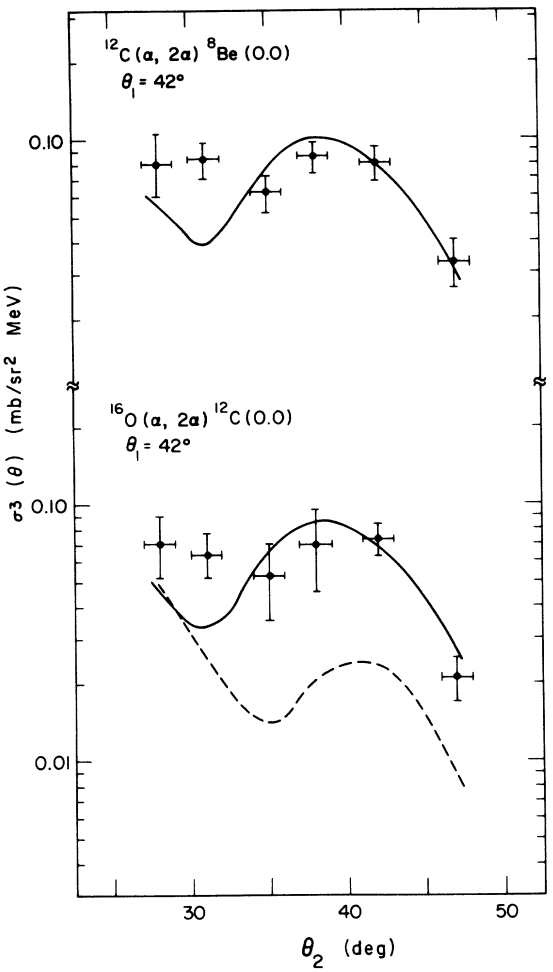

FIG. 7. Asymmetric angular correlations leading to the ground states of ^{8}Be and ^{12}C from the ^{12}C$(\alpha, 2\alpha)$ and ^{16}O$(\alpha, 2\alpha)$ reactions. The $(E_{\alpha\alpha})_i$ prescription is given by the dashed curve; the $(E_{\alpha\alpha})_f$ prescriptions are given by the solid curves.

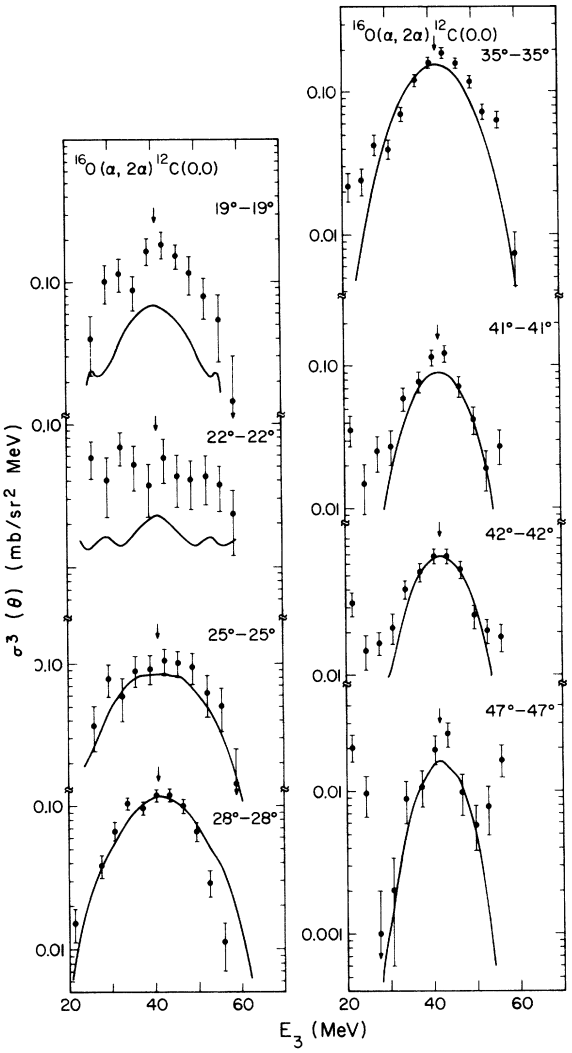

FIG. 8. Energy correlations (as a function of symmetric angle) for the ^{16}O$(\alpha, 2\alpha)^{12}$C(0.0) reaction. The arrows indicate the point at which $E_3 = E_4$.

$$\sigma^3(\theta) = \frac{d^3\sigma}{d\Omega_3 d\Omega_4 dE_3} = (\mathrm{KF})\sigma_{\alpha\alpha}(E_{\alpha\alpha}, \theta)(S_\alpha)_{\mathrm{DW}} |\phi^0_{N0}(\vec{\xi})|^2 , \tag{18}$$

where (KF) are known kinematic factors, $\sigma_{\alpha\alpha}(E_{\alpha\alpha}, \theta)$ are the appropriate cross sections for the free α-α collision,[27] and $\phi^0_{N0}(\vec{\xi})$ is Eq. (14) with $(S_\alpha)_{\mathrm{DW}}$ removed from the integral and explicitly displayed. The arguments $E_{\alpha\alpha}$ and θ of $\sigma_{\alpha\alpha}(E_{\alpha\alpha}, \theta)$ are the c.m. kinetic energy and scattering angle of the two α clusters.

The ambiguity in choosing an appropriate energy for the (α, α) scattering has been treated in the past[1] by choosing a c.m. energy equivalent either to the incoming channel $[(E_{\alpha\alpha})_i]$ prescription or outgoing channel $[(E_{\alpha\alpha})_f]$ prescription. Figure 4 shows the ^{16}O$(\alpha, 2\alpha)^{12}$C(0.0) data compared with the DWIA $(E_{\alpha\alpha})_i$ (dashed curve) and $(E_{\alpha\alpha})_f$ (solid curve) predictions. The $(E_{\alpha\alpha})_f$ choice gives a much better fit, in agreement with results of Ref. 1. The prediction of the minimum at 22° in the angular correlation was insensitive to the β and γ parameters of the distorted waves. A deep minimum in $\sigma_{\alpha\alpha}(E_{\alpha\alpha}, \theta)$ accounts for the minimum in the $(\alpha, 2\alpha)$ correlation at 22° only if the $(E_{\alpha\alpha})_f$ prescription is used.

The angular correlation to the ^{12}C first excited state in Fig. 6 also shows the characteristic minimum at 22°, and reveals that this feature of the impulse approximation theory is present even in the weak excited state transitions. Figure 7 shows the asymmetric angular correlations for the ^{16}O and ^{12}C targets. Again, the $(E_{\alpha\alpha})_f$ prescription

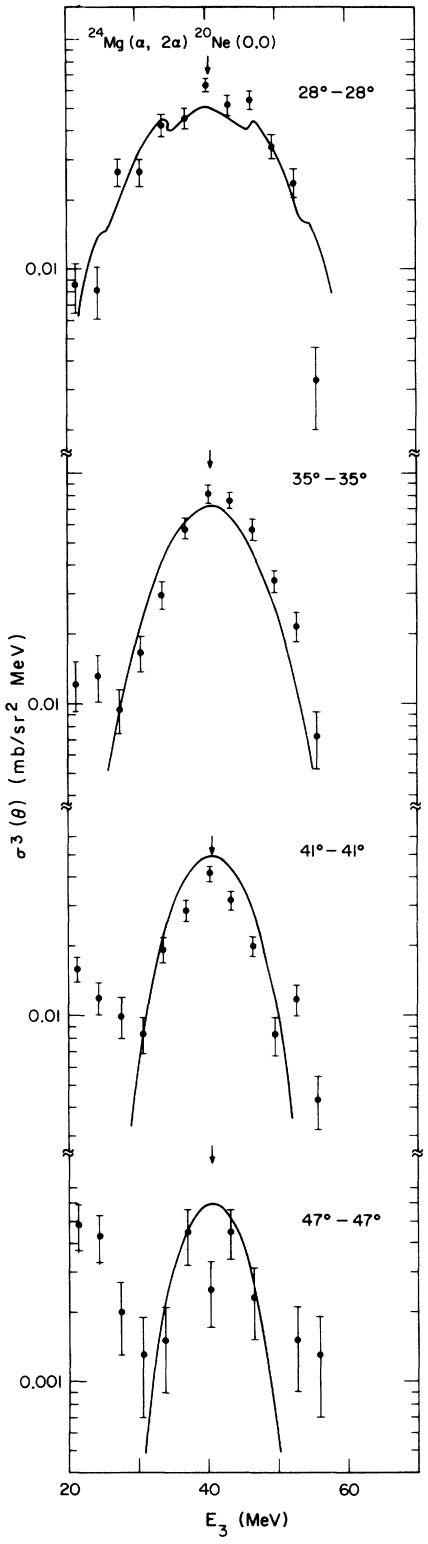

FIG. 9. As in Fig. 8 for the ^{24}Mg target.

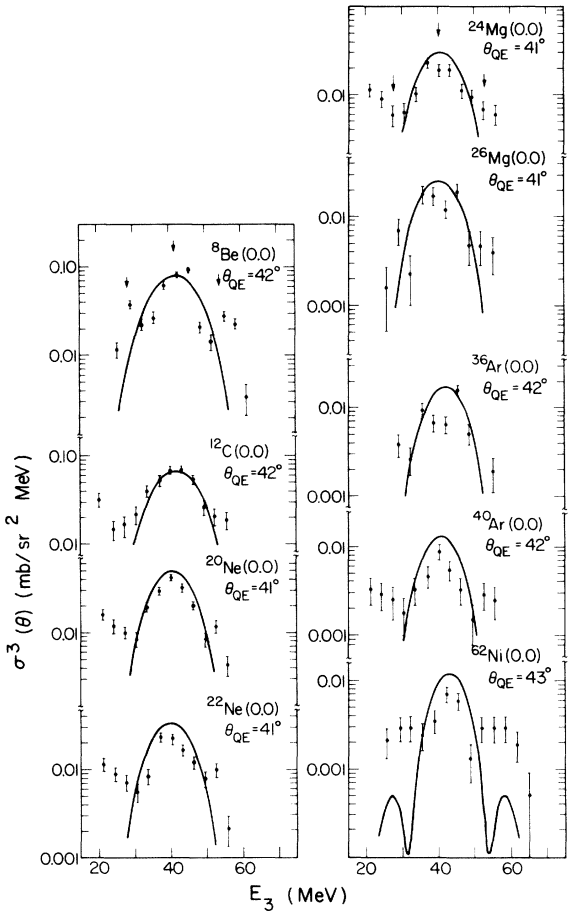

FIG. 10. Energy correlations at the quasielastic (QE) angle for all targets studied in this work. The three arrows correspond to points of zero and 0.6 fm^{-1} recoil momenta ($E_3 < E_4$ and $E_3 > E_4$).

(solid curve) gives the best fit to the ^{16}O($\alpha, 2\alpha$)-^{12}C(0.0) data. On the basis of these results, as well as experience from previous ($\alpha, 2\alpha$) experiments, the $(E_{\alpha\alpha})_f$ prescription has been adopted in this work.

2. *Determination of distortion parameters*

Very little work concerning evaluation of the distortion parameters for these analytic distorted waves has been reported in the literature. Our initial effort in finding a reasonable set was guided by using α-particle optical model potentials[28-31] in Eqs. (10) and (11) to yield starting parameters. Then these parameters were varied to obtain a best fit to the ^{16}O($\alpha, 2\alpha$)^{12}C(0.0) angular correlation data. A reasonably unique distortion parameter set was found which gave $(S_\alpha)_{DW} = 3.0$ for the ^{12}C target,[26,32] i.e., an α particle sum rule was invoked in order to limit an ambiguity found in a search on the $\gamma_1, \gamma_{3,4}$ absorption parameters. This ambiguity

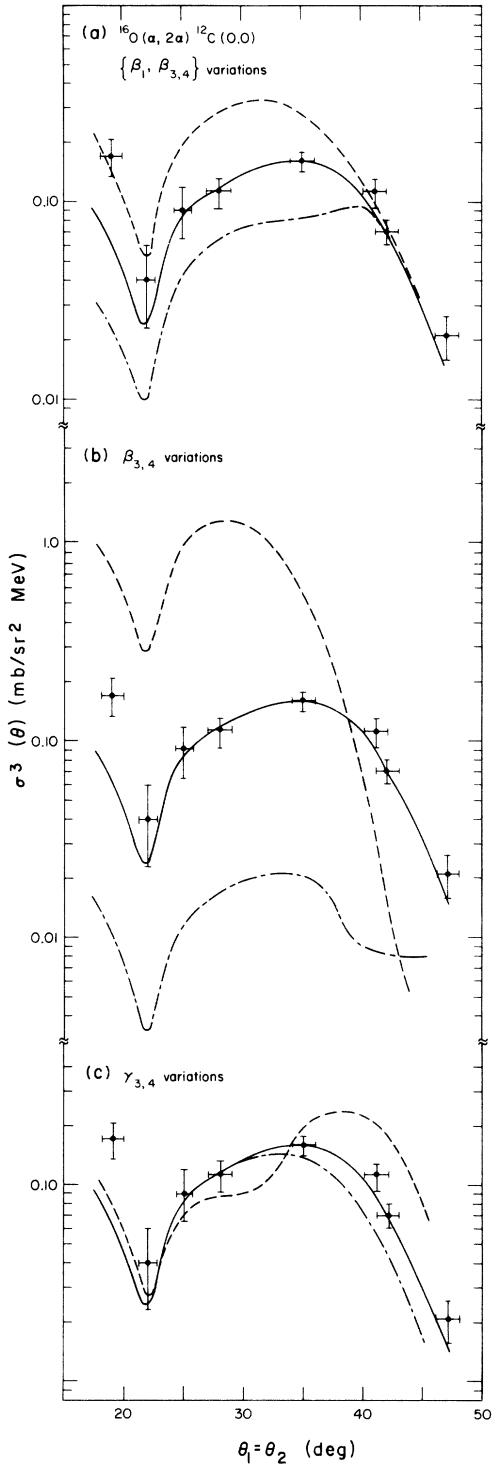

FIG. 11. (a) Effect of varying the pair $(\beta_1, \beta_{3,4})$ on theoretical predictions for $^{16}O(\alpha, 2\alpha)^{12}C(0.0)$. (b) As in (a) except only $\beta_{3,4}$ is varied. (c) As in (a) except $\gamma_{3,4}$ is varied. See text for detailed discussion.

will be discussed in more detail below.

A more satisfactory procedure for distortion parameter determination became available with the publication[17] by Janus and McCarthy (JM) of a systematic survey of (α, α') inelastic scattering using these analytic distorted waves. Our distortion parameters are simply related to theirs, i.e.,

$$\beta_{SHZ} = 1 + \beta_{JM}, \qquad \gamma_{SHZ} = (\gamma k R_N)_{JM}. \tag{19}$$

The subscript *SHZ* has been used for our definition of β and γ. Using Eq. (19) and an averaged β_{JM} and $(\gamma k R_N)_{JM}$ from Table I of Ref. 17 a very good fit to the $^{16}O(\alpha, 2\alpha)^{12}C(0.0)$ angular correlation was found with the distortion parameter set $\{\beta_1, \gamma_1, \beta_{3,4}, \gamma_{3,4}\} = \{0.92, 1.10, 0.94, 1.20\}$ with $(S_\alpha)_{DW} = 2.9$. This normalization is about 20% less than the $(S_\alpha)_{DW}$ computed with the "fit" parameters reported in Refs. 26 and 32; the curves shown in Figs. 4–10 used the parameter set based on the (α, α') scattering[17] listed above. There was no need to adjust distortion parameters with increasing mass in order to maintain good fits. The $(S_\alpha)_{DW}$ are listed in Table IV and will be discussed in more detail in Sec. IV C. Since $\beta_{SHZ} \approx 0.9$, the total potential is repulsive [see Eq. (10)] and the Coulomb potential is apparently playing a major role.[17]

Figure 7 shows the ^{16}O, $^{12}C(\alpha, 2\alpha)$ asymmetric angular correlation predictions using the symmetric angular correlation distortion parameter set given above. The normalization of Fig. 7 is identical to that used in Fig. 4 and is also listed in Table IV. Agreement between the asymmetric angular correlation predictions and data is fair with the worst disagreement occurring at small angles. It is in this angular region that the two outgoing α particles have the greatest asymmetry in energy sharing, and our assumption about equal final state distortion parameters may be inappropriate.

We now turn to a brief discussion of the distortion parameter sensitivity in fitting the $^{16}O(\alpha, 2\alpha)$-$^{12}C(0.0)$ angular correlation data. The energy correlation calculations are not very sensitive to parameter variations. In Fig. 11 variations of three types are presented; all theoretical calculations are normalized by $(S_\alpha)_{DW} = 2.9$. In all cases the solid curve corresponds to the final distortion parameter set discussed in the preceding paragraphs. Similarly, if a parameter is not varied it also equals the previously discussed value. In Fig. 11(a), the $(\beta_1, \beta_{3,4})$ are varied as a pair. The dashed curve corresponds to $(\beta_1, \beta_{3,4}) = (0.62, 0.64)$ and the dot-dashed curve has $(\beta_1, \beta_{3,4}) = (1.22, 1.24)$. Some shape sensitivity is noted, but the best shape fit is given by $(\beta_1, \beta_{3,4}) = (0.92, 0.94)$. Figure 11(b)

shows $\beta_{3,4}$ variations. The dashed curve has $\beta_{3,4}=0.80$ and the dot-dashed curve has $\beta_{3,4}=1.08$. Large changes in both shape and magnitude are noted. These calculations along with results in Fig. 11(a) demonstrate that β_1 and $\beta_{3,4}$ should be approximately equal if a satisfactory shape fit is to be obtained. Figure 11(c) shows the effect of $\gamma_{3,4}$ variations. The dashed curve has $\gamma_{3,4}=0.90$ and the dot-dashed curve has $\gamma_{3,4}=1.50$. For a satisfactory shape fit $\gamma_{3,4}>\gamma_1$. As long as this relation is maintained γ_1 or $\gamma_{3,4}$ could be varied over a considerable range without large shape changes, although the magnitude would change. This is the ambiguity alluded to at the beginning of this section.

Summarizing, it is encouraging that the (α, α') inelastic scattering and the $(\alpha, 2\alpha)$ data can be simultaneously fitted with these analytic distorted waves using essentially the same distortion parameters. However, we do recognize that the agreement of theory with experiment may be fortuitous, since the DWIA is a gross simplification of Eq. (3).

3. *Bound state wave functions*

Two prescriptions were used to describe the bound state radial wave function $R_{N0}(\rho)$ introduced in Eq. (16). Both harmonic oscillator wave functions and Woods-Saxon wave functions calculated by the separation energy procedure[33] were used in data analysis. The number of radial nodes (N) was determined by using Eq. (17). There was little difference in the angular correlation predictions, although the Woods-Saxon wave function did give a slightly better shape fit with constant distortion parameters. Figure 12 compares the $^{16}O(\alpha, 2\alpha)$-$^{12}C(0.0)$ calculations based on the two models; the lack of sensitivity to the bound state radial wave function is shown. The finite well radial wave functions were used for all calculations. Table I provides a summary of the input parameters for $L=0$. The fourth column gives the α particle separation energies and the last column gives the potential depth binding the α cluster derived from the separation energy procedure. The radius and diffuseness parameters which define the Woods-Saxon well shape were taken to be $1.30A^{1/3}$ fm and 0.73 fm, respectively.

Several calculations were performed using $N=0$ rather than N derived from Eq. (17). These angular correlation results were inferior to those given by determining N from Eq. (17). A complete search on the distortion parameters for $N=0$ did not improve the fits.

The effect of radial cutoffs in $R_{N0}(\rho)$ was investigated for the $^{16}O(\alpha, 2\alpha)^{12}C(0.0)$ case. Only small changes in the predicted angular correlation shape

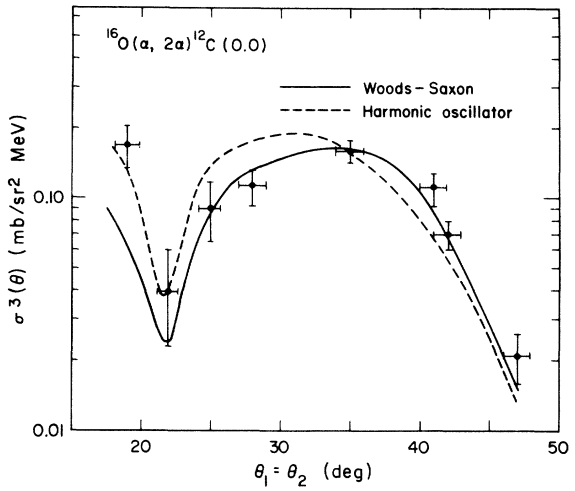

FIG. 12. Comparison of harmonic oscillator and Woods-Saxon bound state wave functions used in the DWIA calculation for the $^{16}O(\alpha, 2\alpha)^{12}C(0.0)$ case.

and magnitude were noted up to a cutoff radius (ρ_c) of 2.5 fm [ρ(surface) $=1.3A^{1/3}=3.275$ fm]. The magnitude decreased by a factor of 2 for $\rho_c=3.80$ fm, but the shape remained nearly unchanged. Similar calculations were done for the PWIA case where it was found that the magnitude decreased monotonically with increasing cutoff radius. This result is expected, since there is no absorption in the PW model, and thus all nuclear radii contribute.

4. *Energy correlations*

Energy correlations for a fixed angular setting were obtained by measuring the cross section for unequal energies of the two outgoing α particles; the E_3 bins were approximately 3 MeV wide. The energy correlations for $^{16}O(\alpha, 2\alpha)^{12}C(0.0)$ and $^{24}Mg(\alpha, 2\alpha)^{20}Ne(0.0)$ as a function of symmetric angle are given in Figs. 8 and 9. The solid curves are the DWIA predictions which utilized the distortion parameters and $(S_\alpha)_{DW}$ found in fitting the angular correlation data (cf. Sec. IV B 2). The DWIA theory correctly predicts the energy correlation broadening as the detector angular separation is reduced. This effect is due to the behavior of the distorted wave part of the calculation. Even though the $\sigma_{\alpha\alpha}(E_{\alpha\alpha}, \theta)$ become flatter as a function of E_3 as the separation angle is increased, $|\phi_{N0}(\vec{\xi})|^2$ becomes relatively more peaked. The PWIA failed to reproduce this observation. The energy correlation results shown in Figs. 8 and 9 were representative of all the nuclei studied.

Figure 10 shows the energy correlations at the quasielastic angle for all the targets studied. The solid curves are DWIA predictions determined

TABLE IV. Spectroscopic information derived from the present $(\alpha, 2\alpha)$ data by use of PWIA and DWIA. The last four columns give pertinent data and clustering predictions from the literature.

Residual nucleus	E_x (MeV)	$(S_\alpha)_{PW}$ PWIA	$(S_\alpha)_{DW}$ (symmetric) DWIA	$(S_\alpha)_{DW}$ (asymmetric) DWIA	$(p, p\alpha)$ relative cross sections	$(^3He, ^7Be)$ [a] relative experimental spectroscopic factor	Theoretical α clustering predictions Ref. 4	Ref. 42
^8Be	0.0	2.9 ± 0.4	2.4 ± 0.4	2.4 ± 0.40	1.0 [b]	0.3	0.674	0.557
	2.90	2.8 ± 0.3			0.6			0.713
^{12}C	0.0	2.9 ± 0.5	2.9 ± 0.4	2.9 ± 0.4	1.0 [c]	1	0.295	0.235
	4.44	0.70 ± 0.23			0.4			1.301
^{20}Ne	0.0	1.05 ± 0.18	1.3 ± 0.2					
	1.63	0.38 ± 0.12						
^{22}Ne	0.0	0.53 ± 0.09	0.83 ± 0.17					
	1.28	0.13 ± 0.05						
^{24}Mg	0.0	0.53 ± 0.12	0.83 ± 0.18			0.3	0.0044	
	1.37	0.19 ± 0.06						
^{26}Mg	0.0	0.38 ± 0.12	0.67 ± 0.19					
	1.81	0.12 ± 0.06						
^{36}Ar	0.0	0.38 ± 0.09	0.91 ± 0.12			0.2	0.0043	
	1.97	0.22 ± 0.07						
^{40}Ar	0.0	0.24 ± 0.09	0.53 ± 0.09					
^{62}Ni	0.0	0.58 ± 0.18	0.83 ± 0.10					
	1.17	0.10 ± 0.05						

[a] See Ref. 4.

[b] See Ref. 6.

[c] See Ref. 40.

from parameters of Sec. IV B 2. The arrows at the E_3 extrema correspond to recoil momenta of 0.6 fm^{-1}. It is noted that for $|\vec{q}| > 0.6$ fm^{-1} the DWIA calculation fails to fit the data; indeed the secondary maxima in the DWIA energy correlations underestimate the data by a factor of 10 at larger $|\vec{q}|$ [cf., the $^{66}Zn(\alpha, 2\alpha)$ case in Fig. 10]. This failure may be due to contributions of nonquasifree type reaction mechanisms which apparently yield a cross section of about 2–10 $\mu b/sr^2$ MeV in these kinematic regions.

C. α cluster spectroscopy by the $(\alpha, 2\alpha)$ reaction

1. Ground and first excited state transitions: PWIA predictions

In this section α cluster spectroscopy of the ground and first excited state transitions will be derived on the basis of the PWIA theory. The following section will be concerned with the DWIA spectroscopic conclusions. Our analytic DW model has been applied only to the ground state transitions, whereas a recent DWIA calculation[34] without this restriction will also be discussed.

The concept of an effective number of α clusters $(S_\alpha)_{PW}$ is introduced through the PWIA relation[6]

$$(S_\alpha)_{PW} = 4\pi \int_0^\infty |\phi(-\vec{q})|^2 q^2 dq \,. \tag{20}$$

It is noted that $(S_\alpha)_{PW}$ is not extracted by normalizing a PWIA calculation to the data, but rather is an integral over the PW momentum distribution. The $|\phi(-\vec{q})|^2$ is extracted from the experimental data using Eq. (18) where $\vec{\xi}$ is replaced with $-\vec{q}$; the analysis is restricted to the ground and first excited states in the residual nuclei. The upper integration limit in Eq. (20) was restricted to $|\vec{q}|$ less than 0.6 fm^{-1}, since reaction mechanisms other than quasifree scattering may be dominating kinematic regions of larger $|\vec{q}|$. The derived $(S_\alpha)_{PW}$ values are given in column 3 of Table IV, and the errors reflect the counting statistics. The $(S_\alpha)_{PW}$ have been normalized to $(S_\alpha)_{DW}$ at the $^{12}C(0.0)$ residual nucleus.

Figure 13 shows results of $(S_\alpha)_{PW}$ versus residual mass for the ground and lowest excited ($J^\pi = 2^+$) levels. There is a strong decrease in $(S_\alpha)_{PW}$ from ^{12}C to ^{30}Si then it is relatively constant to ^{66}Zn. The $(^3He, ^7Be)$ reaction on ^{92}Zr and ^{93}Nb targets and the $(d, ^6Li)$ reaction on ^{114}Sn also revealed leveling of α pickup cross sections for heavier nuclei.[35] A systematic $(d, ^6Li)$ study[36] on targets from ^{12}C to ^{238}U found an over-all cross section decrease proportional to $(A_t)^{-3}$ where A_t is the target mass, but with maxima or minima superimposed on this curve. A comparison of the $(d, ^6Li)$ cross sections with this $(\alpha, 2\alpha)$ work (cf., Table III) shows that the

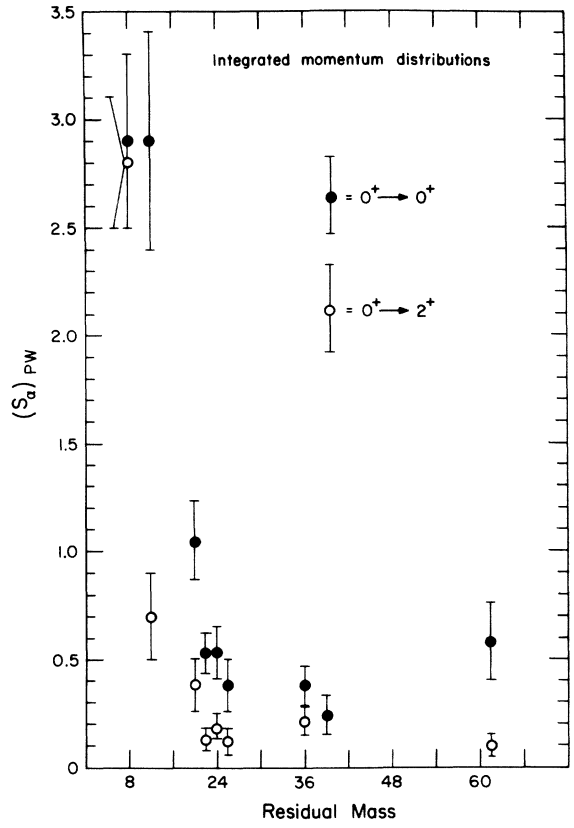

FIG. 13. The effective number of α clusters $(S_\alpha)_{PW}$ vs the residual mass A. Both the ground state and first excited state $(S_\alpha)_{PW}$ are plotted.

$(\alpha, 2\alpha)$ cross sections follow the $(d, {}^6\mathrm{Li})$ cross sections over the mass region in common to both experiments.

The ^{12}C and ^{16}O nuclei have been studied experimentally and theoretically in terms of cluster structure. Table IV (column 6) lists relative excitation strengths derived from the $^{12}\mathrm{C}(p, p\alpha)^8\mathrm{Be}$ experiment at 160 MeV.[6] The results are in fair agreement with the $(\alpha, 2\alpha)$ results. The $({}^3\mathrm{He}, {}^7\mathrm{Be})$ (Ref. 4) and $(d, {}^6\mathrm{Li})$ (Refs. 37 and 38) α pickup reactions on ^{12}C excite the ground and first excited states of ^{8}Be with about the same strength; thus the α knockout and α pickup experimental systematics for the ^{12}C target are similar. α pickup reactions on ^{16}O have found the ^{12}C(4.44) to be 3 or 4 times more strongly populated than ^{12}C(0.0). The $^{16}\mathrm{O}(\alpha, {}^8\mathrm{Be})$ reaction[39] also populated the first excited ^{12}C state more strongly. These pickup results are quite unlike the α knockout experiments, which have shown that ^{12}C(0.0) is more strongly populated than ^{12}C(4.44) [approximately a factor of 4 in the $(\alpha, 2\alpha)$ reaction at $E_\alpha = 90$ MeV and about a factor of 2.5 in the $(p, p\alpha)$ reaction at $E_p = 160$ MeV].[40] Numerous calculations[41-43] (e.g., column 9 of Table IV) have predicted that the dominant parent of ^{16}O in an α cluster model is the $[{}^{12}\mathrm{C}(4.44) + \alpha]$ rather than the $[{}^{12}\mathrm{C}(0.0) + \alpha]$ configuration. This difference suggests that the α knockout and α pickup reactions may not be equivalent probes for finding four particle clusters in nuclei, and it is particularly difficult to understand since the α pickup and α knockout reactions, as noted above, are reasonably consistent for the ^{12}C target.

Another study[44] suggested that the $(d, {}^6\mathrm{Li})$ reaction may be strongly influenced by multistep processes, thus confusing a direct α particle pickup interpretation. This conclusion was reached to a large extent on the basis of a systematic population of unnatural parity states. The $(\alpha, 2\alpha)$ data showed only slight population of unnatural parity states, although all levels above the ground and first excited states were very weak.

We might expect the clustering estimates to be more reliable for neighboring nuclei such as in the $N = Z$ and neutron excess nuclei. If the $(S_\alpha)_{PW}$ are summed for transitions to the 0^+ and 2^+ states, it is seen that the ^{24}Mg result is enhanced by a factor of about 2.5 when compared with ^{26}Mg, and that the ^{28}Si value is 1.4 times greater than ^{30}Si. Finally, ^{40}Ca is enhanced by more than a factor of 2 when compared with ^{44}Ca. The last result is interesting, since larger α clustering in ^{40}Ca over ^{44}Ca was invoked[45] in order to explain the enhanced[46] elastic α scattering at backward angles from ^{40}Ca.

2. *Ground state transitions: Analytic DWIA predictions*

Table IV also summarizes the DWIA normalization constants $(S_\alpha)_{DW}$ extracted from the data using the distortion parameters of Sec. IV B 2. One distortion parameter set has been used for all nuclei. These $(S_\alpha)_{DW}$ were obtained by normalizing the theoretical angular correlations to the experimental data; the fits are shown in Figs. 4 and 5. Table IV also includes the $(S_\alpha)_{DW}$ for asymmetric angular correlations with the distortion parameters found in Sec. IV B 2 and serves to emphasize the consistency in analysis of the data (cf., Fig. 7). The errors given with the S_α are limits indicating where the visual fit of theory to data was noticeably worse. Relative agreement between the DWIA analysis $(S_\alpha)_{DW}$ and the PWIA analysis $(S_\alpha)_{PW}$ is found; this is encouraging, since the $(S_\alpha)_{DW}$ depend on the angular correlation data and the $(S_\alpha)_{PW}$ depend on the energy correlation data at the quasielastic angle.

The relative experimental spectroscopic factors from the $({}^3\mathrm{He}, {}^7\mathrm{Be})$ reaction[4] are given in column 7 of Table IV. They agree well with the $(\alpha, 2\alpha)$ normalizations except for the ^{12}C target. Column 8 gives theoretical predictions for the mass depen-

dence of α clustering based on simple shell model wave functions[4]; the theory does not provide sufficient clustering as the nuclear mass increases. However, a $(d, {}^6\mathrm{Li})$ study[38] with finite range DWBA analysis did obtain spectroscopic factors in agreement with those calculated from wave functions similar to those used in Ref. 4. Thus the question of whether there is more α clustering as a function of mass than predicted by the extreme single particle model remains ambiguous, although the current $(\alpha, 2\alpha)$ analysis suggests that the simple shell model configurations are not sufficient.

A recent DWIA analysis[34] which uses optical model potentials to derive the distorted waves has been used to analyze the $^{16}\mathrm{O}(\alpha, 2\alpha)$ ground and first excited state transitions. This treatment seems to have resolved the puzzle of the $^{16}\mathrm{O}$ parentage discussed in the previous section, as they[34] have found $(S_{2^+})_{\mathrm{DW}}/(S_{0^+})_{\mathrm{DW}} = 8$, in reasonable agreement with theory and α pickup reactions. Given this result, a crucial test of the DWIA theory would be to analyze the $^{12}\mathrm{C}(\alpha, 2\alpha)^8\mathrm{Be}$ reaction, since the PWIA analysis is consistent with theory and α pickup experiments in this case.

V. SUMMARY

The $(\alpha, 2\alpha)$ reaction at $E_\alpha = 90$ MeV has been studied for selected target nuclei from $^{12}\mathrm{C}$ to $^{66}\mathrm{Zn}$. Sufficient energy resolution [250–300 keV (full width at half maximum)] has permitted identification of several low-lying excited states. The ground state to ground state transitions are generally dominant. Most systematic features of the symmetric and asymmetric angular correlations and energy correlations for the ground state transitions have been described by a phenomenological DWIA model. In particular, certain features of the angular correlations have indicated a preference for the $(E_{\alpha\alpha})_f$ prescription (post representation) for selecting the proper free α-α scattering cross sections for use in the DWIA calculation. Inclusion of distortion effects drastically reduced the predicted cross sections from the PWIA. Spectroscopic factors for the ground state transitions were extracted using the DWIA $(S_\alpha)_{\mathrm{DW}}$ and PWIA models $(S_\alpha)_{\mathrm{PW}}$.

The amount of α clustering decreased with the same mass dependence as found in a $({}^3\mathrm{He}, {}^7\mathrm{Be})$ experiment.[4] Both the $({}^3\mathrm{He}, {}^7\mathrm{Be})$ α pickup and $(\alpha, 2\alpha)$ knockout reactions showed that the relative clustering does not decrease as rapidly as predicted by calculations using simple shell model wave functions. This does not preclude the possibility that mixed configuration shell model wave functions contain sufficient α-particle correlations to explain our data.

The relative spectroscopic values were consistent between the PWIA and DWIA treatments. The values extracted using the PWIA were used to compare the relative excitation strengths in the $^{24,26}\mathrm{Mg}$, $^{28,30}\mathrm{Si}$, and $^{40,44}\mathrm{Ca}$ target pairs. The results can be interpreted to mean that the $N = Z$ nuclei have enhanced clustering when compared to the neutron excess partner.

A comparison of the residual levels populated by the $(d, {}^6\mathrm{Li})$ and $({}^3\mathrm{He}, {}^7\mathrm{Be})$ reactions with the $(\alpha, 2\alpha)$ experiments shows that the α knockout reactions strongly select ground state transitions whereas the α pickup reactions do not. This feature is particularly marked to the $^{16}\mathrm{O}$ target, where the pickup reactions find the $^{12}\mathrm{C}(4.44)$ MeV state enhanced by a factor of 3 to 4 compared with the ground state, while the reverse is found in α knockout experiments. This apparent anomaly of the knockout reaction was shown to be a consequence of distortions,[34] and emphasizes the danger of relying too heavily on data analysis via PWIA.

This work has shown the feasibility of using the $(\alpha, 2\alpha)$ reaction at a moderate beam energy as a spectroscopic tool over a broad mass region. Theoretical treatment of the α knockout reaction when compared to an α pickup reaction is quite primitive. Although certain experimental features show that impulse approximation theories have some validity, a more complete theoretical treatment of the reaction process must be given before reliable clustering spectroscopic factors can be extracted. The complementary nature of the results from the two reactions, however, leads us to believe that efforts to improve the theory would be well rewarded.

ACKNOWLEDGMENTS

For aid in the experimental work we acknowledge C. Ellsworth for target preparations, and Dr. D. Kovar and Dr. F. Becchetti for help in collecting the data. Theoretical suggestions were made by Dr. A. Giorni, Dr. F. Becchetti, and Dr. P. Deutchman. We also thank N. S. Chant for sending us his DWIA results prior to publication. We wish to express our thanks for the support of the Los Alamos Scientific Laboratory for one of us (JDS) during the preparation of the paper. Finally, we thank Dr. B. G. Harvey for his support and suggestions given throughout this work.

†Work performed under the auspices of the U.S. Energy Research and Development Administration.

*Present address: Carnegie-Mellon University, Los Alamos Meson Physics Facility, Los Alamos, New Mexico 87545.

[1]H. B. Pugh, J. W. Watson, D. A. Goldberg, P. G. Roos, D. I. Bonbright, and R. A. J. Riddle, Phys. Rev. Lett. 22, 408 (1969); P. Gaillard, M. Chevallier, J. Y. Grossiord, A. Guichard, M. Gusakow, and J. R. Pizzi, *ibid.* 25, 593 (1970); A. Guichard, M. Chevallier, P. Gaillard, J. Y. Grossiord, M. Gusakow, J. R. Pizzi, and C. Ruhla, Phys. Rev. C 4, 700 (1971).

[2]J. W. Watson, H. G. Pugh, P. G. Roos, D. A. Goldberg, R. A. J. Riddle, and D. I. Bonbright, Nucl. Phys. A172, 513 (1971).

[3]I. E. McCarthy and D. L. Pursey, Phys. Rev. 122, 578 (1961).

[4]C. Detraz, H. H. Duhm, and H. Hafner, Nucl. Phys. A147, 488 (1970).

[5]H. D. Holmgren, in *Proceedings of the International Conference on Clustering Phenomena in Nuclei, Bochum, Germany, 21–24 July, 1969* (International Atomic Energy Agency, Vienna, Austria, 1969), p. 17.

[6]B. Gottschalk and S. Kannenberg, Phys. Rev. C 2, 24 (1970).

[7]M. B. Epstein, D. J. Margaziotis, N. S. P. King, and T. A. Cahill, Phys. Rev. C 9, 581 (1974).

[8]R. A. Kenefick, J. W. Watson, G. J. Mroz, and R. Donovan, Texas A&M Progress Report, 1971 (unpublished), p. 15.

[9]L. S. Rodberg and R. M. Thaler, *Introduction to the Quantum Theory of Scattering* (Academic, New York, 1967), p. 202.

[10]M. Jain, P. G. Roos, H. G. Pugh, and H. D. Holmgren, Nucl. Phys. A153, 49 (1970).

[11]B. Mithra and R. Laverriere, Nucl. Phys. A184, 321 (1972).

[12]I. E. McCarthy, Rev. Mod. Phys. 37, 388 (1965).

[13]V. V. Balashov and D. V. Meboniya, Nucl. Phys. A107, 369 (1968).

[14]G. Jacob and Th. A. J. Maris, Rev. Mod. Phys. 38, 121 (1966).

[15]A. J. Kromminga and I. E. McCarthy, Nucl. Phys. 31, 678 (1962).

[16]P. A. Deutchman and I. E. McCarthy, Nucl. Phys. A112, 399 (1968); A. K. Chatterjee and P. A. Deutchman, *ibid.* A189, 20 (1972).

[17]R. T. Janus and I. E. McCarthy, Phys. Rev. C 10, 1041 (1974).

[18]L. J. Denes, W. W. Daehnick, and R. M. Drisko, Phys. Rev. 148, 1097 (1966).

[19]M. Bedjidian, M. Chevallier, J. Y. Grossiord, A. Guichard, M. Gusakow, J. R. Pizzi, and C. Ruhla, Nucl. Phys. A189, 403 (1972).

[20]R. E. Hintz, F. B. Selph, W. S. Flood, B. G. Harvey, F. G. Resmini, and E. A. McClatchie, Nucl. Instrum. Methods 72, 61 (1969).

[21]L. R. B. Elton and D. F. Jackson, Phys. Rev. 155, 1070 (1967).

[22]D. F. Jackson, Phys. Rev. 155, 1065 (1967).

[23]F. S. Goulding, D. A. Landis, and R. H. Pehl, UCRL Report No. UCRL-17560, 1967 (unpublished).

[24]L. B. Robinson, F. Gin, and F. S. Goulding, Nucl. Instrum Methods 62, 237 (1968).

[25]R. D. Plieninger, W. Eichelberger, and E. Velton, Nucl. Phys. A137, 20 (1969).

[26]J. D. Sherman, Lawrence Berkeley Laboratory Report No. LBL-1690, 1973 (unpublished).

[27]R. Nilson, R. O. Kerman, G. R. Briggs, and W. Jentschke, Phys. Rev. 104, 1673 (1956); D. J. Bredin, W. E. Burcham, D. Evans, W. M. Gibson, J. S. C. McKee, D. J. Prowse, J. Rotblat, and J. N. Snyder, Proc. R. Soc. London A251, 143 (1959); H. E. Conzett, G. Igo, H. C. Shaw, and R. J. Slobodrian, Phys. Rev. 117, 1075 (1960); T. A. Tombrello and L. S. Senhouse, Phys. Rev. 129, 2252 (1963); P. Darriulat, G. Igo, H. G. Pugh, and H. D. Holmgren, Phys. Rev. 137, B315 (1965).

[28]H. Rebel, G. W. Schweimer, G. Schatz, J. Specht, R. Lohken, G. Hauser, D. Habs, and H. Klewe-Nebenius, Nucl. Phys. A182, 145 (1972).

[29]G. Hauser, R. Lohken, G. Nowicki, H. Rebel, G. Schatz, G. Schweimer, and J. Specht, Nucl. Phys. A182, 1 (1972).

[30]G. R. Satchler, Nucl. Phys. 70, 177 (1965).

[31]E. P. Lippincott and A. M. Bernstein, Phys. Rev. 163, 1170 (1967).

[32]J. D. Sherman, D. L. Hendrie, and M. S. Zisman, in Contributions to the Second International Conference on Clustering in Nuclei, Univ. of Maryland, College Park, Maryland, 1975 (unpublished).

[33]Code DWUCK, P. D. Kunz (private communication).

[34]N. S. Chant and P. G. Roos, in Proceedings of the Second International Conference on Clustering in Nuclei, Univ. of Maryland, College Park, Maryland, 1975 (unpublished).

[35]C. Detraz, C. D. Zafiratos, H. Rudolph, and C. S. Zaidins, Phys. Rev. Lett. 28, 117 (1972); P. Martin, J. B. Viano, J. M. Louseaux, and Y. Le Chaloney, Nucl. Phys. A212, 304 (1973).

[36]F. D. Becchetti, L. T. Chua, J. Jänecke, and A. M. VanderMolen, Phys. Rev. Lett. 34, 225 (1975).

[37]R. L. McGrath, D. L. Hendrie, E. A. McClatchie, and B. G. Harvey, Phys. Lett. 34B, 289 (1971).

[38]H. Gutbrod, Y. Yoshida, and R. Bock, Nucl. Phys. A165, 240 (1971).

[39]G. J. Wozniak, N. A. Jelley, and J. Cerny, Phys. Rev. Lett. 31, 607 (1973).

[40]S. L. Kannenberg, Ph.D. thesis, 1968 (unpublished).

[41]P. Beregi, N. S. Zelenskaja, V. N. Neudatchin, and Yu. F. Smirnov, Nucl. Phys. 66, 513 (1965).

[42]D. Kurath, Phys. Rev. C 7, 1390 (1973).

[43]H. H. Gutbrod, H. Yoshida, and R. Bock, in *Nuclear Reactions Induced by Heavy Ions*, edited by R. Bock and W. R. Hering (North-Holland, Amsterdam, 1970).

[44]J. R. Comfort, W. J. Braithwaite, J. R. Duray, H. T. Fortune, W. J. Courtney, and H. G. Bingham, Phys. Lett. 40B, 456 (1972).

[45]N. C. Schmeing, Nucl. Phys. A142, 449 (1970).

[46]G. Gaul, H. Ludecke, R. Santo, H. Schmeing, and R. Stock, Nucl. Phys. A137, 177 (1969).